MEBT-BI-SC91-04

Technical Design of the MEBT Scrappers

A. R. Páramo A. Vizcaíno I. Bustinduy

14 June 2017

Project: MEBT
Version: 0.4
Approved by: I. Bustinduy
Revised by: G. Bakedano, F. Sordo

Change History

Rev.	Date	Author(s)	Description
0.1	2017-04-05	A. R. Páramo	First Version
0.2	2017-05-30	A. R. Páramo	Minor modifications
0.3	2017-06-14	A. R. Páramo	Document Revision
0.4	2017-06-14	I. Bustinduy	Document Revision

Technical Design of the MEBT Scrappers

A. R. Páramo[1*], A. Vizcaíno[1], I. Bustinduy[1]

[1] Accelerator/Control & Diagnostics Group, ESS-Bilbao, Spain

[*]Corresponding author: arparamo@essbilbao.org

1. Introduction

In this work, we study the behaviour of the MEBT Scrapper under operational conditions expected in the ESS-MEBT.

In Figure 1 the position of the scrappers in the MEBT Layout is shown and in Figure 2 we show a sketch with the design of the scrapper. This preliminary design shows the TZM plate that withstands irradiation using a support of a steel cooled body. The connection of the steel body to the actuator depends on the required instrumentation; measured charge signal will be collected, for which the steel body and cooling channels need to be insulated from the actuator.

In Table 1 we describe the technical requirements for the MEBT Scrappers as agreed on "L4_MEBT_ID_20161101_ID.xlsx". For the ESS MEBT scrapper, the requirement has been set in scrapping 0.25 % of the beam per blade, or 625 W of peak beam power. The beam parameters for the design are σ_x=2.5 mm and σ_y=0.9 mm. Which roughly correspond to the beam parameters of the Scrapper 3, where the beam is more focused and leads to more detrimental effects. In Table 2 we summarize the design and operational parameters for the MEBT Scrappers.

The thermomechanical effects of irradiation on the MEBT-Scrapper were studied in previous works [1, 2]. However, the previous works studied operation with tungsten or graphite. Finally, TZM has been chosen as the material for the scrappers due to vacuum constrains. TZM capabilities to withstand thermal shock are similar to tungsten while it is easier to machine. Compared with graphite, TZM do not have proton-material interaction that forms carbides as the case of graphite. Therefore, in this work we study the operation of the TZM scrappers, we also analyse the geometry of the TZM plate and the rest of components of the scrapper.

In this work, we design the components to operate in the elastic regime under nominal operation. We divide the analysis on *i)* study the thermomechanical effects of transient irradiation on the irradiated plate and *ii)* study of operation in the steady state for the different components of the MEBT Scrappers.

The material properties are summarized in Appendix A: Material Properties.

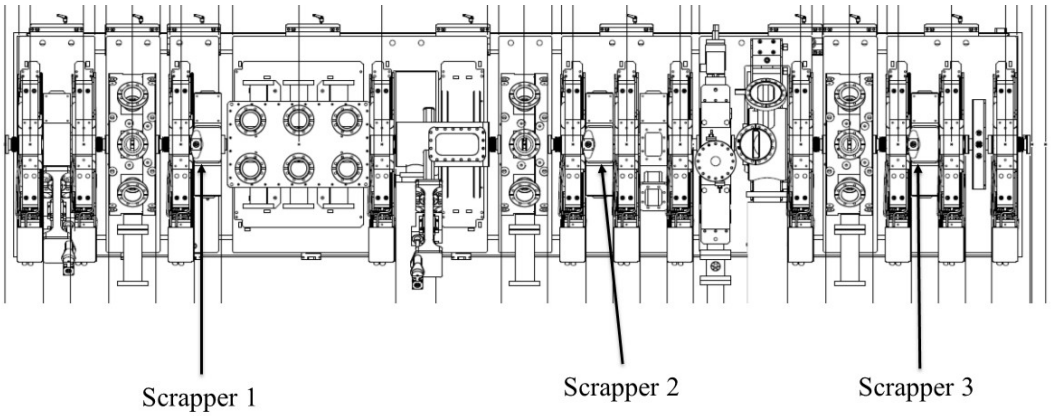

Figure 1: Layout of the ESS-MEBT (ESS-0053289.2).

Table 1: L4 requirements for the MEBT-Scrappers. Requirements from "L4_MEBT_ID_20161101_ID.xlsx"

User Defined ID	Name	Description
MEBT-L4-ID-010	Beam collimator: collimation peak power	Each jaw of the beam scraper shall be able to withstand a minimum peak power of 625 W for the nominal beam duty cycle and pulse length
NEW (20161010)	Beam collimator: beam size at the collimator location	The calculations for the design optimization shall consider a proton beam whose distribution is defined by a bi-Gaussian distribution with similar transverse sizes given by a sigma of 0.9 mm.
MEBT-L4-ID-020	Beam collimator: number and location	Scrapers shall be placed at 3 different locations in the MEBT based on the integrated lattice design
MEBT-L4-ID-030	Beam collimator: position adjustment precision	The scraper jaw transverse position adjustment resolution shall be better than ±50 μm.
MEBT-L4-ID-040	Beam collimator: charge measurement	Each scraper jaw shall be instrumented such as to measure a minimum charge of 1 nano-Coulomb integrated over a period of 50 micro second*
MEBT-L4-ID-050	Beam collimator: jaw translation range	Each scraper jaw shall be movable independently such that its lower part can be located between 2.8 and 20 mm with respect to the beam axis

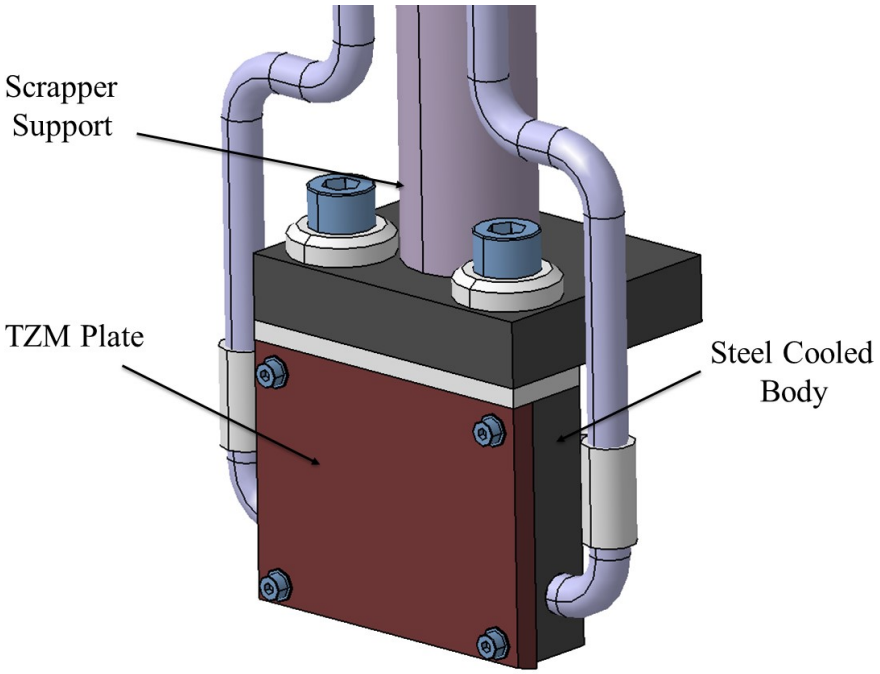

Figure 2: Sketch with the main components of the scrappers.

Table 2: Beam Parameters and irradiation conditions used in this work. Scrappers Requirements according to "L4_MEBT_ID_20161101_ID.xlsx" and scrapper position according to 2015 v0c Layout. The position of the scrapper is referred from the RFQ optical exit.

Parameter	**Value**		**Parameter**	**Value**
Proton Energy	3.63	MeV	Scrapper 1	
Intensity	62.5	mA	Position	862 mm
Frequency	14	Hz	σ_x	1.813 mm
Pulse Duration	2860	μs	σ_y	3.251 mm
			Scrapper 2	
Scrapping Requirement	0.25	%/blade	Position	2324 mm
Scrapping Peak Power	625	W/blade	σ_x	3.114 mm
Scrapping Average Power	24.5	W/blade	σ_y	3.853 mm
			Scrapper 3	
Design Beam Size (σ_x)	2.5	mm	Position	3536 mm
Design Beam Size (σ_y)	0.9	mm	σ_x	2.548 mm
			σ_y	0.986 mm

2. Transient Analysis

In this section, we study the thermomechanical effects of the irradiation pulse in the scrappers. We study the irradiation profile in the scrapper, the scrapper position and its effect on the irradiated material (TZM).

2.1. Model Description

2.1.1. FEM Model

In order to estimate the thermo-mechanical effects of pulse irradiation in the irradiated material we have developed a FEM Model. For the FEM model the heat load is calculated as either a surface load or as a volumetric load using MCNPX calculations.

In Figure 3 we show the Ansys 3D FEM model used in this analysis.

The mesh is refined in the irradiated surface in order to reproduce the Bragg Peak. Regarding mechanical boundary conditions, symmetry conditions and a fixed support in the back of the plate are applied. It is important to point out that the symmetric boundary conditions result in a conservative estimation over models with free surfaces as boundary conditions. Therefore, this model with two symmetry planes represents a conservative estimation of irradiation in the scrappers, where the irradiation is only symmetric in one plane.

Regarding thermal conditions, the analysis studies irradiation on a plate with a uniform temperature of 300 K. No cooling conditions or radiative effects are included, which also results in a conservative estimation.

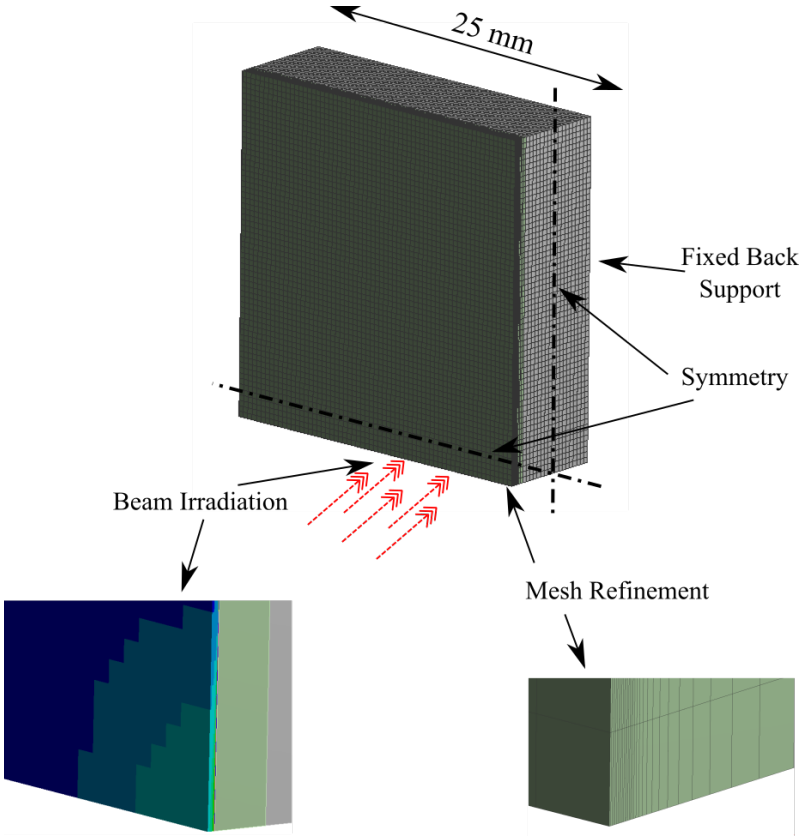

Figure 3: 3D FEM model used in this work.

2.1.2. Heat Load

The beam irradiation follows a Gaussian profile defined by:

$$I''(x,y) = \frac{I_o}{2\pi\sigma_x\sigma_y} \cdot e^{-\frac{x^2}{2\sigma_x^2}} \cdot e^{-\frac{x^2}{2\sigma_y^2}} \quad (1)$$

Where I'' is the current density, I_0 the beam current, σ_x, σ_y the beam standard deviation, and x,y the position from the axis.

In order to calculate the heat load from beam irradiation we use a model using the volumetric heat deposition as calculated from MCNPX. In Figure 4 we show the heat load models.

In Figure 5 we show the stopping power for different irradiated materials. We observe how in copper (GlidCop), TZM and Steel the stopping powers are similar, with penetration ranges of ~50 µm, in graphite the ions penetrate up to ~130 µm, while for tungsten the beam is stopped at ~30 µm.

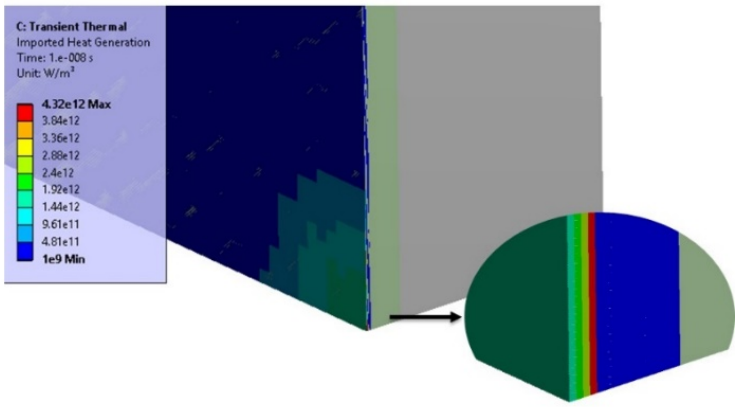

Figure 4: Volumetric heat load as obtained from MCNPX. The figure shows an example for irradiation in tungsten with a beam of 3.63 MeV, 62.5 mA and σ_x=σ_y=2.5 mm.

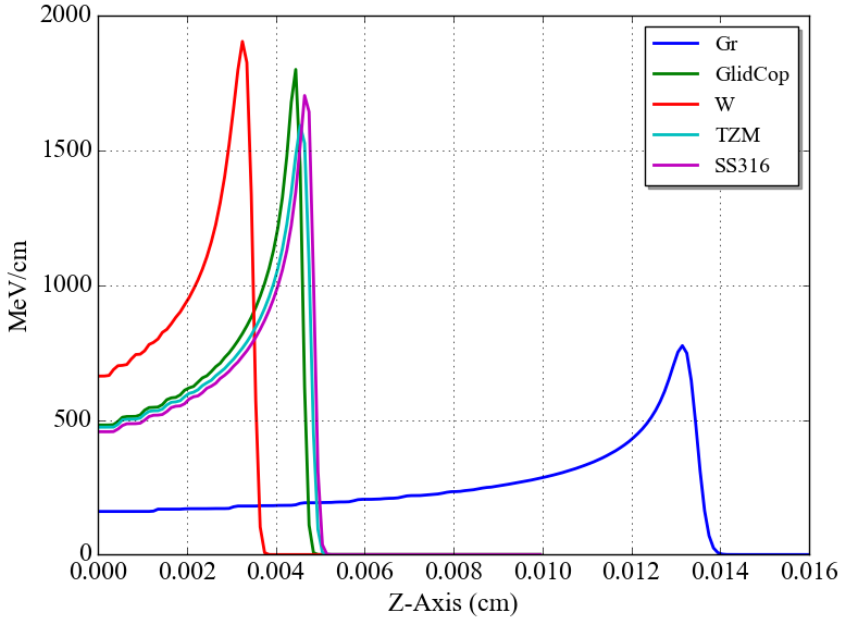

Figure 5: Stopping power for 3.63 MeV protons in different materials.

2.2. Scrappers Irradiation

The power flux (P) in the scrapper and the scraped power ($P_{scrapped}$) correspond to (see also Appendix C: Scrapped Beam Estimation):

$$P = \frac{I \cdot E}{2\pi\sigma_x\sigma_y} \cdot e^{-\frac{x^2}{2\sigma_x^2}-\frac{y^2}{2\sigma_y^2}} \quad (2)$$

$$P_{scrapped} = \mathrm{I} \cdot \mathrm{E} \cdot \frac{1}{2}\left(1 - \mathrm{erf}\left(\frac{x^*}{\sqrt{2}\cdot\sigma_x}\right)\right) \quad (3)$$

Where I is the beam intensity, E the proton energy and σ the beam size.

The design conditions for the MEBT scrappers are σ_x=2.5 mm, σ_y=0.9 mm and a scrapped power of $P_{scrapped}$=625 W (see Table 2). This corresponds to a scrapper insertion of x^*=6.94 mm for a vertical scrapper and y^*=2.5 mm for a horizontal scrapper.

In Table 3 we summarize the beam position for the scrappers for an scrapped power of 625 W or 0.28% of the beam. Irradiation on a perpendicular scrapper would lead to a power flux of 341 MW/m^2. This flux is too high and would lead to stresses much higher than the yield strength of the material. In order to minimize the irradiation effects, the irradiation should incise in the scrapper with an inclination angle.

For an inclination angle of 15º, in Table 4 we show the results for the design conditions σ_x=2.5 mm, σ_y=0.9 mm. We observe how in this case the stresses are ~429 MPa, below the yield strength of the material. In Figure 6 we show the temperature evolution during the first irradiation pulse and in Figure 7 we show the temperature, stresses and strains for the scrapper placed in horizontal position.

It is important to point out that the design condition position should not be exceeded. In Figure 8 we show the beam flux and beam power as function of the position from the axis centre. We observe that small variation in the scrapper position would lead to a great increase in the scrapped power. Therefore, the position x^*=6.94 mm, y^*=2.5 mm should not be exceeded. Even small insertions of 50-100 μm would increase the power flux and the stresses in a ~30%, leading to much quicker material degradation.

Table 3: MEBT Scrappers position in order to scrap 625 W of 0.28 % of beam power. The calculations show scrappers with an inclination angle of 15º.

Component	σ_x (mm)	σ_y (mm)	x^* (mm)	y^* (mm)	P (MW/m^2)	$P_{scrapped}$ (W)	$P_{scrapped}$ (%)
Scrapper 1	1.813	3.251	5.04	9.04	33	625	0.28 %
Scrapper 2	3.114	3.853	8.66	10.71	16		
Scrapper 3	2.548	0.986	7.08	2.74	78		
Scrapper Design	2.5	0.9	6.94	2.50	88		

Table 4: Thermomechanical results for scrapper insertion. The results show the design conditions σ_x=2.5 mm, σ_y=0.9 mm for an inclination angle of 15º.

Case	x^* (mm)	y^* (mm)	P (MW/m^2)	$P_{scrapped}$ (W)	$P_{scrapped}$ (%)	ΔT (K)	σ_{VM} (MPa)	σ_{yield} (MPa)	$\sigma_{VM}/\sigma_{yield}$
3D Vertical	6.94	-	88	625	0.28%	261	429	681	63%
3D Horizontal	-	2.50	88	625	0.28%	240	408	685	60%

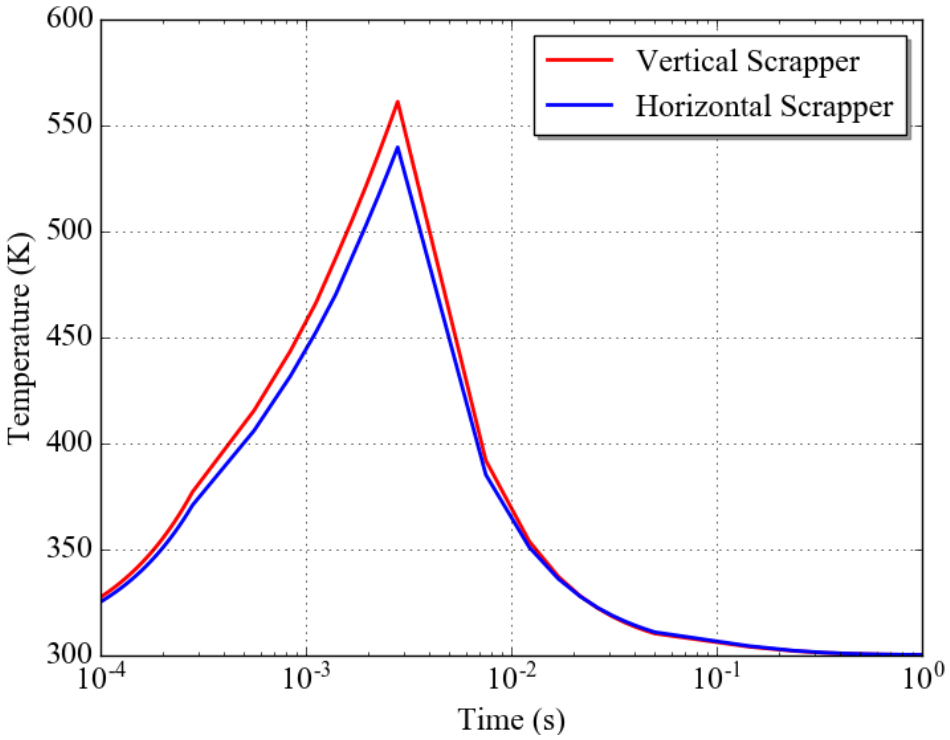

Figure 6: Temperature evolution in the irradiated TZM for the horizontal and vertical scrapper. The results show the design conditions σ_x=2.5 mm, σ_y=0.9 mm for an inclination angle of 15º.

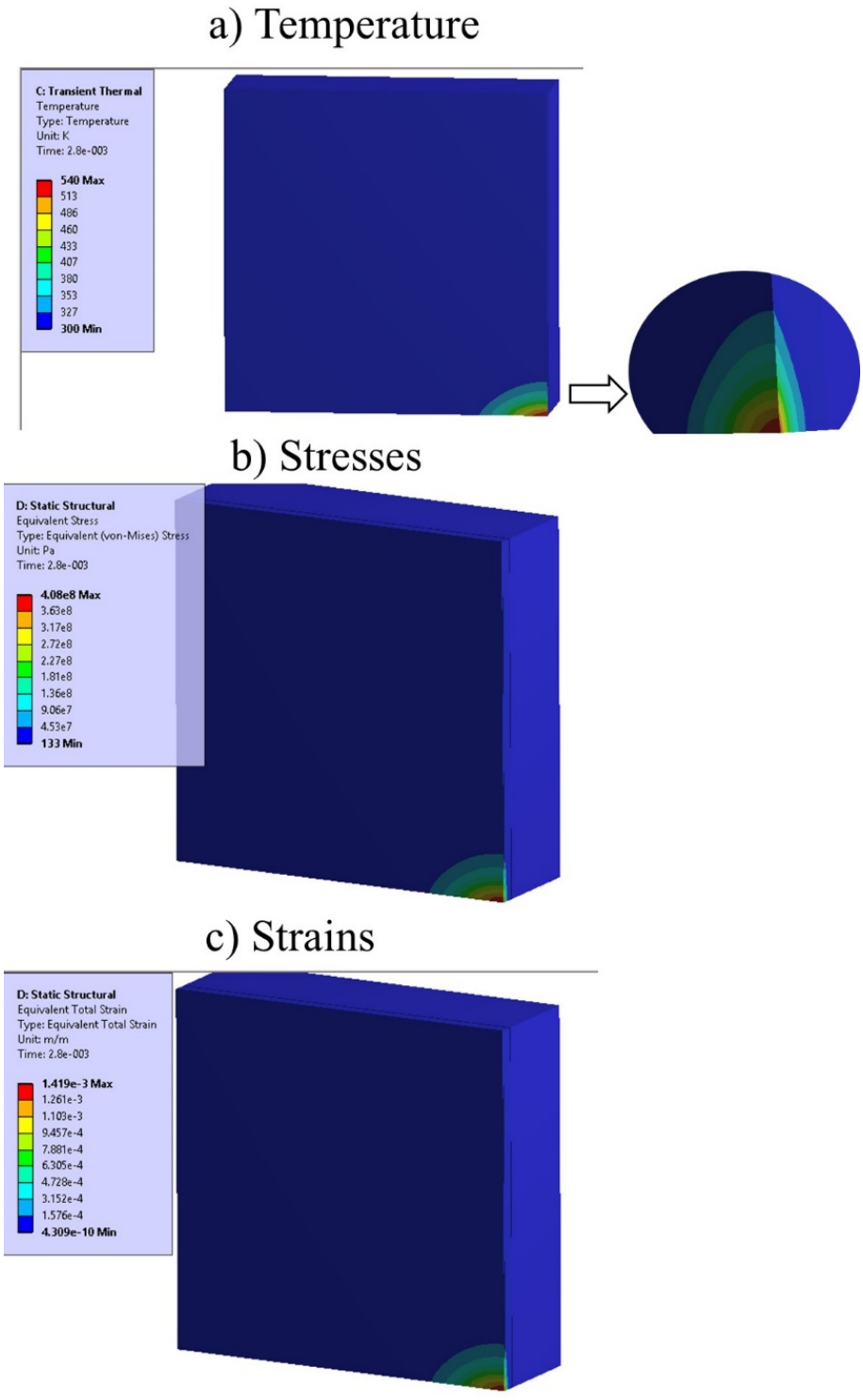

Figure 7: Thermomechanical results after the pulse transient for the horizontal scrapper. The results show the design conditions σ_x=2.5 mm, σ_y=0.9 mm for an inclination angle of 15º.

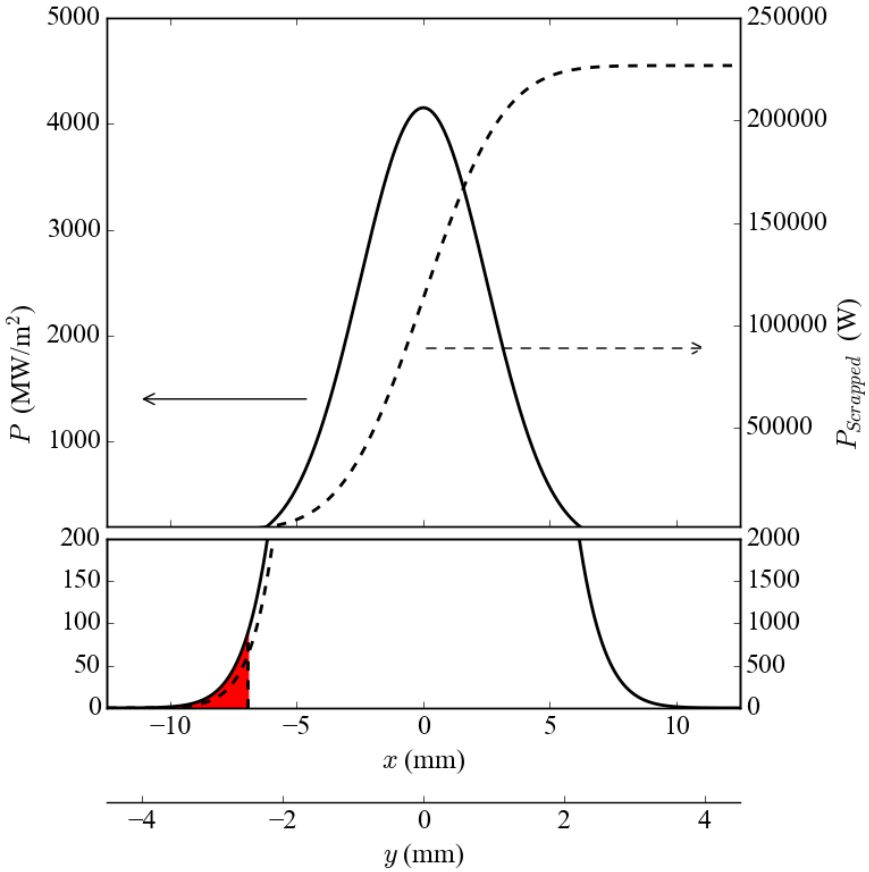

Figure 8: Beam power flux (straight lines) and beam power (dashed) as function of the distance to the axis centre: x for vertical scrappers and y for horizontal scrappers. The red area shows the scrapped beam in the design position x^*=6.94 mm, y^*=2.5 mm.

2.3. **Vessel Irradiation**

When irradiation arrives to an inclined surface, part of it is backscattered. In order to estimate the scattered flux, we simulate the beam irradiation in the scrappers.

In Table 5 we show the values of back scattered irradiation for a 3.63 MeV proton beam in TZM for different irradiation angles as calculated with MCNPX. We show the values of maximum irradiation at 5 mm from the scrapper, with maximum values of ~5 MW/m^2 for angles of 5º, fluxes ~1 MW/m^2 for angles of 10º and ~0.1 MW/m^2 for angles of 15º. The scattered flux depends on the beam shape, therefore there are small differences between the scrappers in horizontal and vertical positions. In Figure 9 we show the flux map of the scattered irradiation.

Using a conservative 1D model (see Section Appendix B: 1D FEM Model) we estimate the thermomechanical response in the steel vessel for pulses of 2.8 ms. In Table 5 we show the stresses expected if the vessel is placed at 5 mm from the scrappers. We observe that in the case of inclination of 5º, damage is expected if the vessel is placed near the scrapper, with stresses ~200 MPa. For 10º or 15º no problem is expected, since the stresses are much below the yield strength of steel of ~200 MPa.

From this study, we conclude that attention should be paid if scrappers with 5º of inclination are placed. For 10º or 15º correct operation is expected with no effects from backscattered beam on the vessels.

Table 5: Fraction of scattered beam for a 3.63 MeV proton beam in TZM as function of the irradiation angle.

Angle		**Scattered Beam (%)**	**Scattered Energy (%)**	**Scattered Flux at 5 mm P (MW/m^2)**	**Stresses in steel at 5 mm σ_{VM} (MPa)**
90	-	0	0.00%	-	
15	Hor.	0.89%	0.17%	0.2	7
	Ver.			0.1	4
10	Hor.	6.35%	1.91%	0.6	20
	Ver.			0.8	29
5	Hor.	25.62%	12.90%	4.0	141
	Ver.			5.9	211

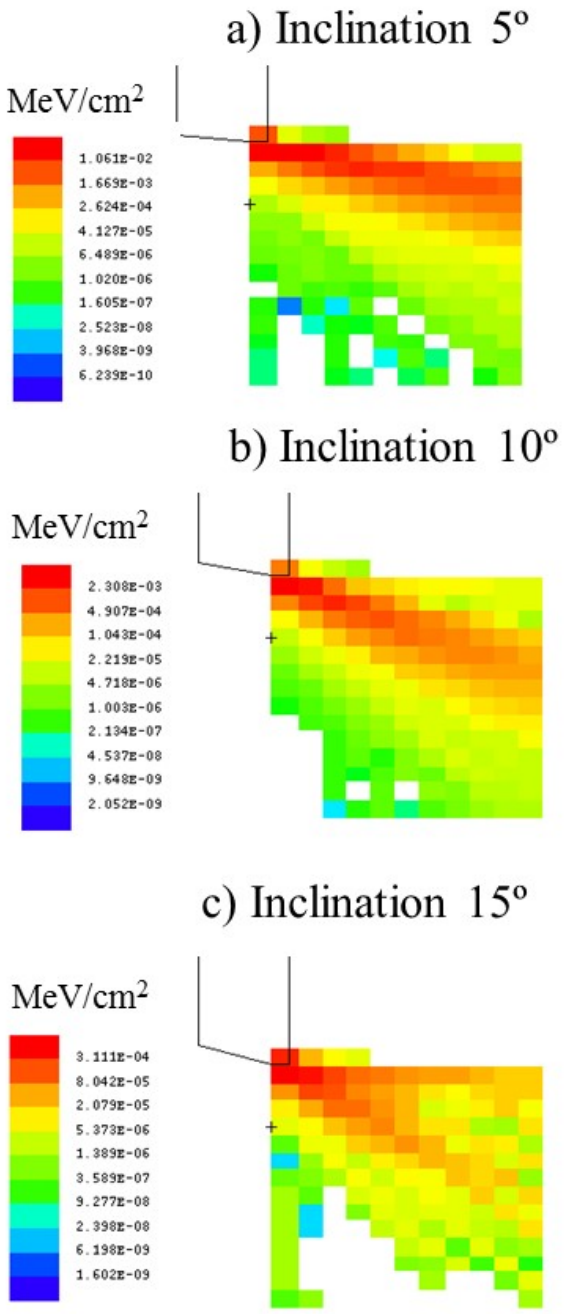

Figure 9: Backscattered irradiation flux for 3.63 MeV protons in the TZM MEBT scrappers for different irradiation angles. The figure shows the scrappers in vertical positions at y^*=2.5 mm for a beam with σ_x=2.5 mm and σ_y=0.9 mm.

3. Steady State Analysis

In this section, we study operation of the scrappers, evaluating how continuous irradiation will lead to a steady state. We study the temperature and stresses in the steady state, and assess that the different components will operate correctly.

3.1. Model Description

In order to study the temperature and stresses during operation we use a FEM model. In the model we include the TZM plate, the steel cooled body and support screws. The geometry of the scrapper is 50x40 mm with a chamfer in the TZM plate of 15º. The TZM plate has a thickness of 10 mm and the steel body of 10 mm. The cooling channels for the steel body have a inner diameter of 4 mm. In Table 6 we summarize the main parameters of the model. In Figure 10 the FEM model for the scrapper is shown.

For the thermal boundary conditions (BD), we characterize irradiation as a surface flux with σ_x=2.5 mm, σ_y= 0.9 mm on an inclined chamfer of 15º. The scrapper is placed at x^*=6.4 mm or 2.5 mm from the beam axis, for the vertical and horizontal scrappers (see Section 2). The average power deposited by the beam is 24.5 W. The initial temperature for the model is 300 K (27ºC). For the joining we assume ideal thermal contact between the TZM and the steel body in the pressed region, and no thermal contact out of this region. The approximation of ideal thermal contact requires that forces ~1000 N are applied to the screws, which is guaranteed by tightening the screws with their nominal torques. For the cooling, we impose a film coefficient of 5000 W m^{-2} K^{-1} and water at 300 K.

Regarding mechanical boundary conditions, we apply a force of 200 N per screw. We assume friction contact between the TZM plate and the steel. We impose a friction coefficient of μ=1.

Table 6: FEM Model of the Steady State.

Component	Value
Irradiated Plate	TZM
Body	Steel
Water Channel Inner Diameter	4 mm
Film Coefficient	5000 W/m2K
Water Temperature	300 K

Parameter	Value
Dimensions	50x40 mm
Inclination	15º
TZM Plate Thickness	10 mm
Steel Body Thickness	10 mm

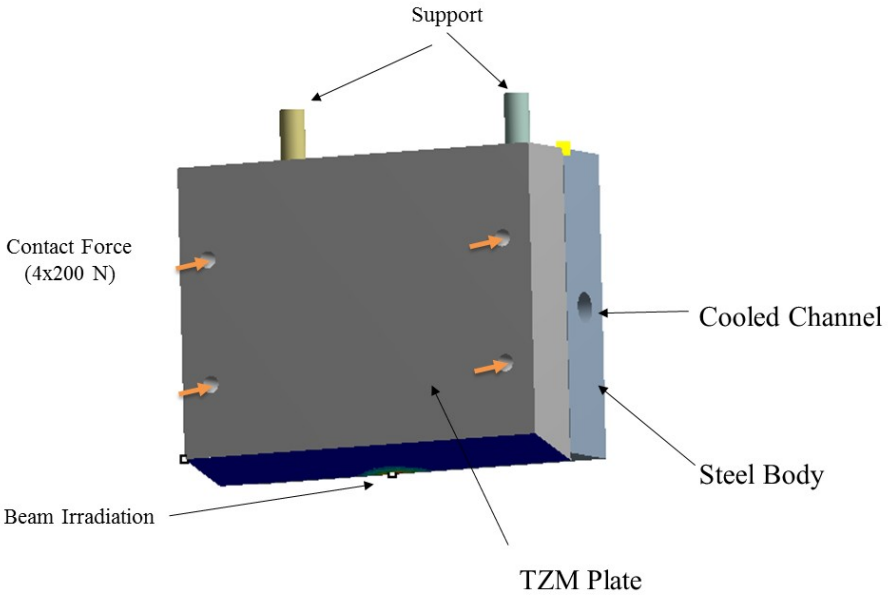

Figure 10: FEM Model for the analysis of the steady state for the Steady State Analysis.

3.2. Cooling System

In this section, we describe the main parameters of the cooling system. We design the cooling system to have good heat transfer conditions with film coefficients of ~5000 W/m^{2}K in cooling channels of 4 mm of inner diameter.

In order to estimate the film coefficient we use Colburn equation [3]:

$$Nu = 0.023 \cdot Re_D^{4/5} \cdot \mathrm{Pr}^{1/3} \quad (4)$$

Where $Nu = h \cdot D/k$ is the Nusselt number, *Re* the Reynolds number and *Pr* the Prandtl number.

The pressure losses can be calculated as:

$$\Delta P = \frac{1}{2}\left(f\frac{L}{D} + K\right) \cdot \rho \cdot v^2 \quad (5)$$

Where *f* is the friction factor, *L* the equivalent pipe length, *D* the pipe diameter, ρ the fluid density, *K* the singular losses and *v* the speed.

In order to have a quick estimation of the friction factor we can use explicit formulations such Haaland [4]:

$$\frac{1}{f^{1/2}} = -1.8 \cdot \log\left(\frac{6.9}{Re_D} + \left(\frac{\epsilon/D}{3.7}\right)^{1.11}\right) \quad (6)$$

Where *f* is the friction factor, *Re* the reynolds number, ϵ is the pipe roughness and *D* the pipe diameter.

In order to have a preliminary estimation we can assume a roughness of ϵ=100 μm, piping length of 2 m and singular losses K~20.

In Table 7 we show the main heat transfer parameters. We observe that in order to obtain a film coefficient ~5000 W/m^{2}K in a channel of ϕ 4 mm we need water flowing at 1 m/s or ~0.75 l/min. For the pressure losses for this system, and we observe that they are in the range of 0.2 bars.

Table 7: Main parameters for the heat transfer and pressure losses of a water cooled channel.

Parameter	Value	Unit	Parameter	Value	Unit
ID	4	mm	*f*	0.06	
v	1	m/s	*L*	2	m
Q	1.75	l/min	$\Delta P_{friction}$	15230	Pa
			K	20	
Re	3988		$\Delta P_{singular}$	9899	Pa
Nu	33				
H	5008	W/m^2 K		25219	Pa
			ΔP	0.25	Bar

3.3. **Results Steady State**

We study the nominal operation mode, with pulses of 2.8 ms irradiating the scrapper at 14 Hz. In total the irradiation has an average power of 24.5 W.

The heat deposited in the TZM plate is evacuated through conduction in the pressed TZM-Steel body surface. Then in the steel body the heat is removed by the cooling channels.

In Figure 11 we show the temperature evolution of the scrapper after the beginning of operation. We observe how the steady state is attained in ~1000 s. In the steady state the TZM plate is heated up to ~140 ºC (410 K).

In Figure 12 we show the temperature, stress and deformations in the steady state. The highest temperatures, see Figure 12 (a), are attained in the irradiated area, TZM plate. For the steel body, the highest temperatures are attained in the regions in contact with the TZM, while the region near the cooled channels are at temperatures near 300 K.

Regarding the stresses, see Figure 12 (b), the temperatures gradient induces compressive stresses in the irradiated region of the TZM. This causes stresses of ~25 MPa in the TZM plate, which is much lower than the stresses due to the thermal shock during the irradiation pulse. In the steel body stresses up to 70 MPa are attained. The highest stresses are attained near the cooling channel due to the temperature gradient, and in the support region. In any case, stresses in the steel body are much lower than yield strength which is ~200 MPa.

Regarding the deformations, see Figure 12 (c), maximum deformations of ~20 μm appear. The analysis of the contact pressure between the TZM plate and the steel body, Figure 12 (d), shows that there is only contact where the force is applied, which corresponds to the washer area.

In Table 8 the results of operation in the steady state are summarized.

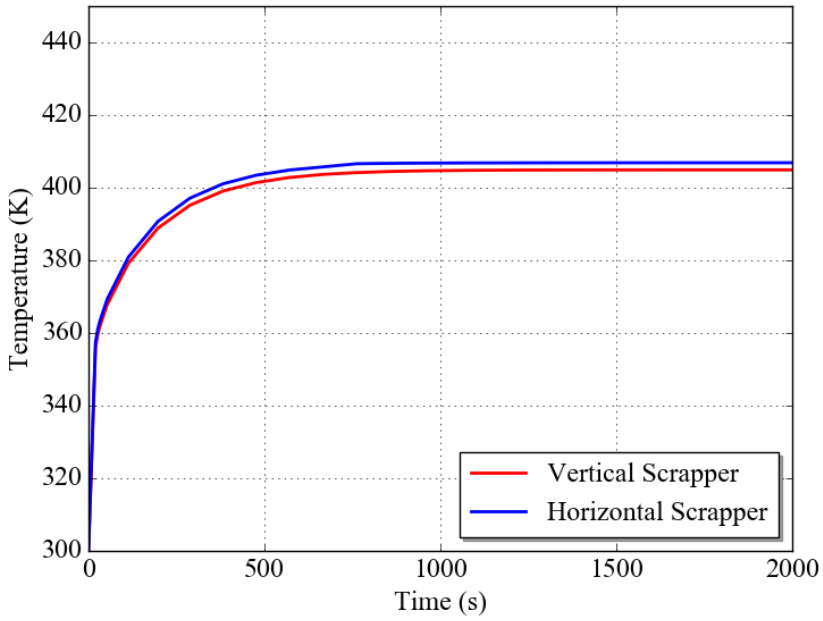

Figure 11: Temperature transient after the start-up.

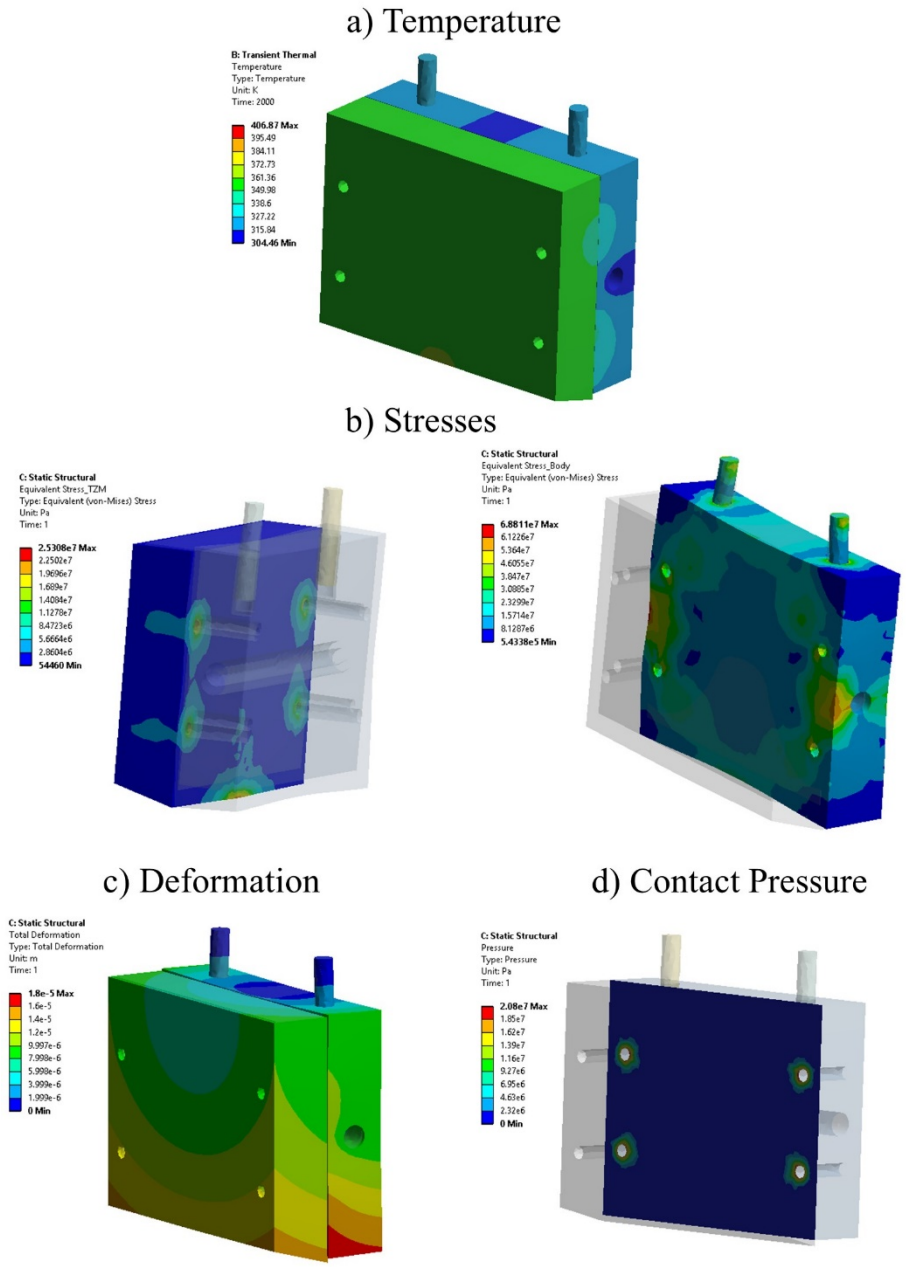

Figure 12: Thermomechanical results in the steady state for the horizontal scrapper.

Table 8: Thermomechanical results in the main components of the scrappers in the steady state.

Case	x^* (mm)	y^* (mm)	$P_{averagecrapped}$ (W)	ΔT (K)	Def. (µm)	σ_{VM} (MPa)	σ_{yield} (MPa)	$\sigma_{VM}/\sigma_{yield}$
Vertical	6.94	-	25	105	18	17.2	720	2%
Horizontal	-	2.50	25	107	18	25.3	719	4%

3.4. Results Transient + Steady

In the steady state the TZM plate will have to withstand irradiation pulses. With the model described in Section 2, we study the transient irradiation effects at the steady state temperature (~130 ºC).

On a first approximation, we can divide the thermo-mechanical effects in the transient and steady cases:

$$\Delta T = \Delta T_{steady} + \Delta T_{transient} \qquad (7)$$

$$\Delta \sigma = \Delta \sigma_{steady} + \Delta \sigma_{\mathrm{transient}}$$

Where T is the temperature and σ the stresses.

In Table 9 we show the thermomechanical effect of irradiation in the steady state. Comparing irradiation at the initial temperature (27ºC) or at the steady state temperature (130ºC) one can observe at higher temperature the lower conductivity leads to slightly higher temperature and stresses, also the yield stress of TZM decreases.

Table 9: Transient effects under irradiation in the steady state.

Case	ΔT max (ºC)	Def (µm)	$\Delta\sigma_{VM}$ (MPa)	σ_{yield} (MPa)	$\sigma_{VM}/\sigma_{yield}$
Horizontal Scrapper					
Initial	27	0	0		
Steady	107	18	25.3	719	4%
Transient 2800 µs (Initial T=27 ºC)	240	-	408	685	60%
Transient 2800 µs (Steady T=134 ºC)	245		430	684	63%
Total 2800 µs (Init. + Steady + Transient)	**379**	**18**	**455**	**665**	**68%**
Vertical Scrapper					
Initial	27	0	0		
Steady	105	18	17.2	720	2%
Transient 2800 µs (Initial T=27 ºC)	261	-	429	681	63%
Transient 2800 µs (Steady T=132 ºC)	267	-	454	679	67%
Total 2800 µs (Init. + Steady + Transient)	**399**	**18**	**471**	**663**	**71%**

3.5. Fatigue Analysis

In this section, we try to define the number of cycles before irradiation damage begins to erode the TZM surface.

The thermomechanical effects of irradiation are characterized by the heating of the irradiated surface and the associated surface expansion and compressive stresses. These effects take place during each irradiation pulse, and over cyclic repetition may give appearance to fatigue effects. The fatigue effects are characterized by surface erosion caused by appearance and propagation of micro-cracks. As a general rule, these effects can be minimized if the material operates in the elastic regime, below the yield strength.

For surface loads, the thermo-mechanical effects depend on the Heat Flux Factor $F_{HF} = P \cdot \tau^{1/2}$. Where P is the heat surface flux and τ the pulse duration. For a 1D model with a surface thermal load, the temperature and stresses can be analytically calculated as [5, 6]:

$$\Delta T_{\mathrm{FHF}} = 2\, P\, \tau^{\frac{1}{2}} (\pi k \rho c)^{-1/2} = 2 \cdot F_{HF} \cdot (\pi k \rho c)^{-1/2} \qquad (8)$$

$$\sigma_{VM} = E\, \alpha \frac{\Delta T}{1-\nu} = \mathrm{E} \cdot \alpha \frac{2\, P\, \tau^{\frac{1}{2}} (\pi k \rho c)^{-\frac{1}{2}}}{1-\nu} = \mathrm{E} \cdot \alpha \frac{2\, F_{HF} \cdot (\pi k \rho c)^{-\frac{1}{2}}}{1-\nu} \qquad (9)$$

Therefore, the thermomechanical effects of irradiation depend on the irradiation conditions characterized by the Heat Flux Factor $F_{HF} = P \cdot \tau^{1/2}$ and the material properties. This analysis is useful to compare the response of different materials and under different irradiation conditions.

We compare the response of TZM and tungsten using a simple 1D FEM model (see Appendix B: 1D FEM Model Description). We estimate the limit for the appearance of plastic effects as ~5 MW m^{-2} s$^{1/2}$ (see Table 10).

In the case of tungsten there is also abundant experimental data of irradiation effects. In Figure 13 we show experimental results for the irradiation campaign carried out by Loewenhoff et al in Ref. [7]. In Ref. [7], for pulses of 0.48 ms and loads of 140 MW/m^2 (F_{HF}=3 MW m^{-2} s$^{1/2}$) no damage is expected for at least 10^6 cycles. While for loads of 270 MW/m^2 (F_{HF}=5.9 MW m^{-2} s$^{1/2}$) damage is expected at around 10^6 cycles.

In the case of tungsten, the effect of temperature on irradiation damage has a great effect [8]. In Ref. [7], the irradiation campaign was done at a temperature of 200 ºC, which is similar to the operational temperature the beam dump in ESS. However, at lower temperatures tungsten may undergo irradiation damage at much lower number of cycles. This is due to is high Ductile-Brittle Transition Temperature (DBTT), which typically is above room temperature [9]. In the case of TZM the effect of temperature is lower, since has a lower DBTT, typically below room temperature [1] [10, 11]

In Table 10 we summarize the irradiation effects, and as expected the experimental data for tungsten shows good agreement with the analytic estimations. Due to their similar behaviour, we expect similar limits for tungsten and TZM, with no damage appearance below F_{HF}~3 MW m^{-2} s$^{1/2}$ and damage at ~10^6 cycles for F_{HF}~5 MW m^{-2} s$^{1/2}$.

[1] The Ductile-Brittle Transition Temperature (DBTT) is highly dependant on grain size, impurities and surface finishing. Therefore it exact value depends on the used material variety.

For the case of the scrappers operation in the ESS MEBT, we have operation with a beam power of ~88 MW/m^2 for pulse duration of 2.86 ms, which means Heat Flux Factors of F_{HF}~4.7 MW m^{-2} s$^{1/2}$.

From this analysis, we conclude that the scraper will be able to operate for ~10^6 cycles withstanding pulses of 2.86 ms before irradiation damage begins to degrade the lower part of the TZM plate.

Table 10: Summary of irradiation limits for tungsten and TZM and comparison with operational conditions expected in ESS MEBT.

Material	F_{HF} **(MW m^{-2} s$^{1/2}$)**	**Comment**
W	5.2	1D FEM Plastic Limit
TZM	4.7	1D FEM Plastic Limit
W	5.9	~10^6 pulses [7]
W	3	>10^6 pulses [7]
TZM	5.3	~10^6 pulses (Estimation)
TZM	2.7	>10^6 pulses (Estimation)
-	4.7	Operation with 2.86 ms in ESS-MEBT

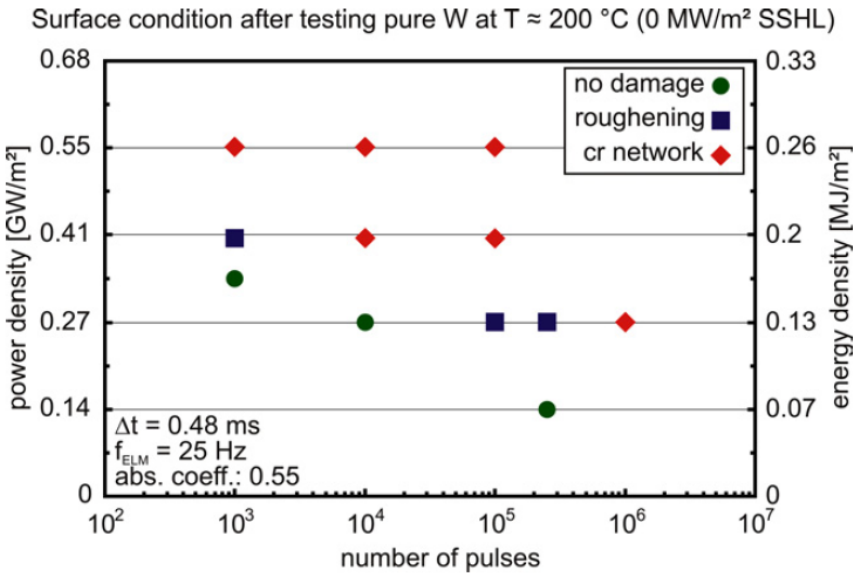

Figure 13: Effects on irradiated tungsten as function of the number of pulses. Figure from Ref. [7].

4. **Conclusions**

In this work, we have evaluated the thermomechanical effects of irradiation in the MEBT scrappers. We study the thermomechanical effects of irradiation, the position of the scrapper, and the heating of the scrapper until the steady state is attained. We performed the analysis for an irradiated TZM and we conclude that the desired operational conditions (625 W-0.25% scrapped per blade) can be obtained using a 15º chamfered TZM plate.

As design recommendations TZM plates of 5 or 10 mm with a 15º chamfer can be used. The scrapper plate should be placed far from the steel components of the beam piper or the vessel, the minimum distance should be larger than 5 mm.

Appendix A: Material Properties

In this work we use Graphite R4550 and tungsten with material properties obtained from Linac 4 CERN Group, and reported in Refs. [12–14]. For TZM we use material properties reported in Refs. [15, 16]. For GlidCop we use properties for GlidCop Al-60 reported in Refs. [17, 18]. For pure copper we use properties reported in Ref. [19] with strength limits from Ref. [20]. For Steel we use SS316L properties reported in Ref. [19] and yield strength reported for SS316 in Ref. [21]. For alumina we use the properties reported in Refs. [20, 22] for Alumina of 99.9% purity.

For the emissivities we use an emissivity for unoxidized copper of 0.02 and 0.28 for polished steel [19]. For TZM we take an emissivity of 0.05 [16, 23].

The material properties of the materials used in the work are summarized in Table 11.

Table 11: Material properties for Graphite R4550 [12, 13], Tungsten [12, 13], TZM [15, 16], GlidCop [17, 18], pure copper [19, 20] and Steel [19, 21] .

Mat. Limit	**Graphite**	**Tungsten**	**TZM**	**GlidCop**	**Pure Copper**	**Steel**	**Alumina**
Max. Temp. (K)	3773	3673	2893	1383	1357	1700	2000
Ult. Tensile Strength (MPa)	40	1425	900	448	209	460	552
Ult. Comp. Strength (MPa)	125	-	-	-			
Yield Strength at 300 K (MPa)	-	1360	750	365	33	206	
Young Modulus (GPa)	11.7	405	310	130	125	200	386
Poisson Coefficient	0.15	0.3	0.31	0.326	0.343	0.3	0.22
Thermal Conductivity at 300 K (W $m^{-1} K^{-1}$)	103	173	119	310	398	14	39
Density at 300 K (kg m^{-3})	1800	19000	10220	8810	8930	7930	3960
Specific Heat at 300 K (J $kg^{-1} K^{-1}$)	824	133	267	391	385	472	880
Coefficient Of thermal expansion at 300 K (μm m-1 K^{-1})	4	5	5	16	16	15	8

Appendix B: 1D FEM Model Description

We use a 1D Ansys FEM model applying plane strain conditions in order to simulate thermomechanical effects of irradiation.

Regarding thermal conditions, we apply a uniform initial temperature of 300 K, the thermal load is either introduced as a surface or volumetric load (see Section 2.1.2) and no radiative effects are included. For the geometry of the model a plate of 3 mm of thickness with a mesh with sizes from 2-10 μm is used.

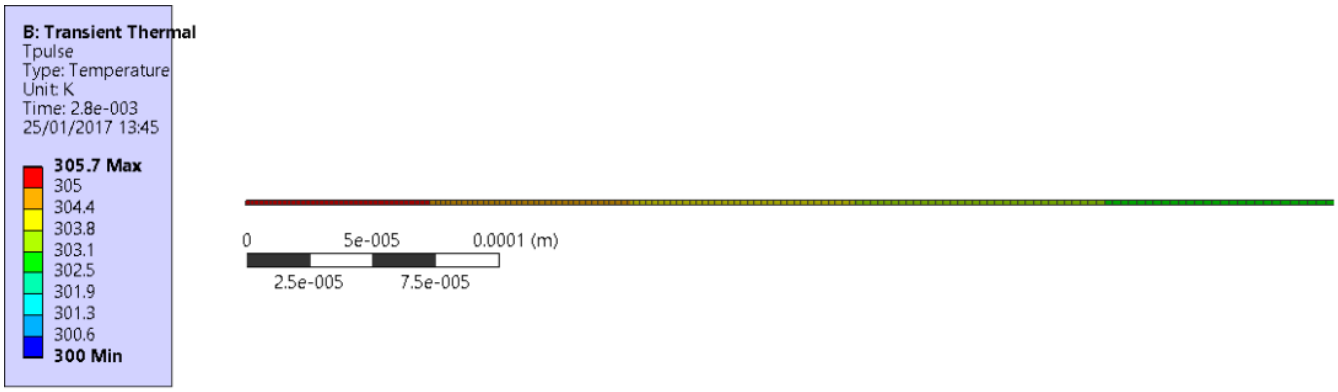

Figure 14: 1D FEM model for the estimation of the thermomechanical effects of the irradiation pulse. The Figure shows the temperature for an example for a pulse of 2.8 ms with powers of 3.54 MW/m^2 on copper.

Appendix C: Scrapped Beam Estimation

In order to study the fraction of collimated beam we integrate the beam tail that would impact on the scrapper. In Figure 15 we show a scheme of the beam profile and the beam fraction that is scrapped.

The irradiation beam can be characterized as a Gaussian profile:

$$I'' = \frac{I_0}{2\pi \cdot \sigma_x \cdot \sigma_y} \cdot e^{-\frac{x^2}{2\sigma_x^2} - \frac{y^2}{2\sigma_y^2}} \quad (10)$$

If the scrapper plate is placed at positions x^*, y^*, the fraction of scrapped beam can be calculated as:

$$I_{scrapped} = \frac{\mathrm{I}_0}{2\pi \cdot \sigma_x \cdot \sigma_y} \cdot \int_{x^*}^{\infty} e^{-\frac{x^2}{2\sigma_x^2}} dx \cdot \int_{y^*}^{\infty} e^{-\frac{y^2}{2\sigma_y^2}} dy \quad (11)$$

If we scrap only in the x direction:

$$I_{scrapped} = \frac{\mathrm{I}_0}{\sqrt{2\pi} \cdot \sigma_x} \cdot \int_{x^*}^{\infty} e^{-\frac{x^2}{2\sigma_x^2}} dx \quad (12)$$

That is the same as:

$$I_{scrapped} = \frac{\mathrm{I}_0}{\sqrt{2\pi} \cdot \sigma_x} \cdot \frac{1}{2}\left(\sqrt{2\pi} \cdot \sigma_x - \int_{-x^*}^{x^*} e^{-\frac{x^2}{2\sigma_x^2}} dx\right) \quad (13)$$

Doing a variable change $t = \frac{x}{\sqrt{2} \cdot \sigma_x}$:

$$I_{scrapped} = \frac{\mathrm{I}_0}{\sqrt{2\pi} \cdot \sigma_x} \cdot \frac{1}{2}\left(\sqrt{2\pi} \cdot \sigma_x - \sqrt{2} \cdot \sigma_x \int_{-\frac{x^*}{\sqrt{2} \cdot \sigma_x}}^{\frac{x^*}{\sqrt{2} \cdot \sigma_x}} e^{-t^2} dt\right) \quad (14)$$

$$I_{scrapped} = \frac{\mathrm{I}_0}{\sqrt{2\pi} \cdot \sigma_x} \cdot \frac{1}{2}\left(\sqrt{2\pi} \cdot \sigma_x - \sqrt{2} \cdot \sigma_x \cdot \sqrt{\pi} \cdot \mathrm{erf}\left(\frac{x^*}{\sqrt{2} \cdot \sigma_x}\right)\right) \quad (15)$$

$$I_{scrapped} = \mathrm{I}_0 \cdot \frac{1}{2}\left(1 - \mathrm{erf}\left(\frac{x^*}{\sqrt{2} \cdot \sigma_x}\right)\right) \quad (16)$$

Where $I_{scrapped}$ is the scrapped beam, x^* is the position of the scrapper, and σ_x, σ_y the beam size.

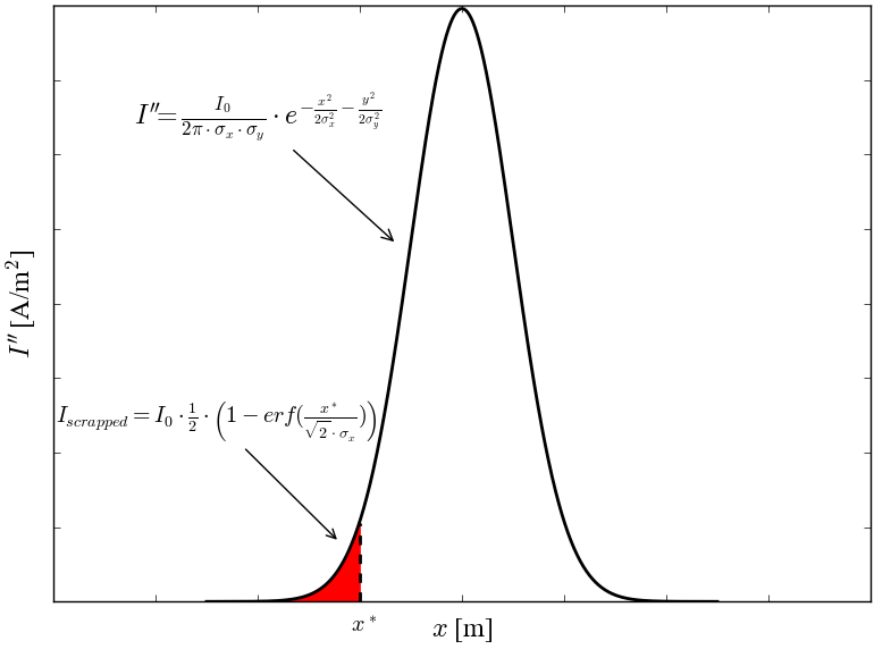

Figure 15: Scheme showing the beam gausian profile and the tail with the beam scrapped fraction (in red).

References

[1] M. Magan and I. Bustinduy, "Basic Scrapper Beam Design analysis," ESS-Bilbao, Internal ESS-Bilbao MEBT-BI-SC01, Jan. 2016.

[2] G. Bakedano, "Basic Scraper Thermomechanical Analysis," ESS-Bilbao, Internal ESS-Bilbao MEBT-BI-SC02, Sep. 2016.

[3] F. P. Incropera, D. P. DeWitt, T. L. Bergman, and A. S. Lavine, *Fundamentals of Heat and Mass Transfer*, Edición: 6th ed. Hoboken, NJ: Wiley John + Sons, 2006.

[4] F. White, *Fluid Mechanics*, 7 edition. New York, N.Y.: McGraw-Hill Education, 2010.

[5] G. G. van Eden et al., "The effect of high-flux H plasma exposure with simultaneous transient heat loads on tungsten surface damage and power handling," *Nucl. Fusion*, vol. 54, no. 12, p. 123010, 2014.

[6] J. H. Yu, G. D. Temmerman, R. P. Doerner, R. A. Pitts, and M. A. van den Berg, "The effect of transient temporal pulse shape on surface temperature and tungsten damage," *Nucl. Fusion*, vol. 55, no. 9, p. 93027, 2015.

[7] T. Loewenhoff et al., "Evolution of tungsten degradation under combined high cycle edge-localized mode and steady-state heat loads," *Phys. Scr.*, vol. T145, p. 14057, Dec. 2011.

[8] J. Linke et al., "Performance of different tungsten grades under transient thermal loads," *Nucl. Fusion*, vol. 51, no. 7, p. 73017, 2011.

[9] J. R. Stephens, "Review of deformation behavior of tungsten at temperature less than 0.2 absolute melting temperature," 1972.

[10] P. Hu et al., "Preparation and ductile-to-brittle transition temperature of the La-TZM alloy plates," *Int. J. Refract. Met. Hard Mater.*, vol. 52, pp. 131–136, Sep. 2015.

[11] Y. Hiraoka, H. Kurishita, M. Narui, and H. Kayano, "Fracture and Ductile-to-Brittle Transition Characteristics of Molybdenum by Impact and Static Bend Tests," *Mater. Trans. JIM*, vol. 36, no. 4, pp. 504–510, 1995.

[12] F. Carra and A. Dallochio, "LINAC4 3MeV test stand: Thermo-mechanical analysis of the Slit," CERN, CERN CH1211 Geneva 23 Switzerland, CERN Internal Report 1102149 0.1, Nov. 2010.

[13] T. Mora, I. Bustinduy, and F. Sordo, "ESS-Bilbao Beam Stoppers criteria (MEBT-BI-FC04-02)," 16-May-2016.

[14] SGL Group: The Carbon Company, "Specialty Graphites for the Metal Industry," SGL Group, Commercial Brochure.

[15] D. Smith, W. Daenner, and Y. Gohar, "ITER blanket, shield and material data base," Oct. 1991.

[16] "Molybdenum | Plansee." https://www.plansee.com/en/materials/molybdenum.html.

[17] SCM Metal Products Inc., "GLIDCOP: Copper Dispersion Strengthtened with Aluminium Oxide." .

[18] Z. Wang, "Thermophisical and Mechanical Properties of Glid-Cop," Argonne National Laboratory, Intra-Laboratory Memo, Jan. 1991.

[19] Y. Lee and M. Hartl, "ESS Target Materials Handbook," Internal ESS ESS-0028465, Feb. 2016.

[20] ASM, *ASM Handbook Volume 2: Properties and Selection : Nonferrous Alloys and Special-Purpose Materials*, 10th edition. Place of publication not identified: ASM International, 1990.

[21] “http://aries.ucsd.edu/LIB/PROPS/PANOS/.” .

[22] “Aluminum Oxide | Al2O3 Material Properties.” http://accuratus.com/alumox.html.

[23] Mikron Instrument Company, “Table of emissivity of various surfaces.” .